Computers and Structures 292 (2024) 107235

Contents lists available at ScienceDirect

Computers and Structures

journal homepage: www.elsevier.com/locate/compstruc

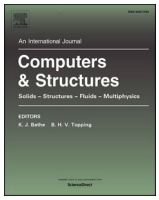

An exact method for free vibration of beams and frameworks using frequency-dependent mass, elastic and geometric stiffness matrices

J.R. Banerjee

School of Science and Technology, City, University of London, Northampton Square, London EC1V 0HB, United Kingdom

ARTICLE INFO

Keywords:
Axially-loaded beams
Free vibration
Frequency-dependent mass, elastic and geometric stiffness matrices
Wittrick-Williams algorithm
Dynamic stiffness method

ABSTRACT

The frequency-dependent mass, elastic and geometric stiffness matrices of an axially loaded Bernoulli-Euler beam are developed through rigorous application of symbolic computation. These three matrices are related to the corresponding dynamic stiffness matrix so that free vibration analysis of axially loaded beams and frameworks can be carried out in an exact manner by applying the Wittrick-Williams algorithm as solution technique. Representative results from the proposed theory are presented for different boundary conditions of beams and frameworks, carrying tensile and compressive loads. Comparative results from finite element method are also presented. The duality between the free vibration and buckling problems is captured in that when the compressive load in a beam or frame approaches its critical buckling load, the fundamental natural frequency tends to zero and thus, buckling can be thoughtfully interpreted as free vibration at zero frequency. The investigation has opened the possibility of including damping in free vibration analysis of beams and frameworks when applying the dynamic stiffness method.

1. Introduction

The original idea of frequency dependency of mass and stiffness matrices of structural elements for free vibration analysis was put forward by Przemieniecki [1] who formulated the frequency dependent mass and stiffness matrices of a beam and provided series expansions of the matrices by retaining two frequency dependent terms. Przemieniecki's work was further developed by subsequent researchers who also relied on power series expansion of the mass and stiffness matrices and truncated the series at some convenient point. For instance, by using dynamic discretisation method, Downs [2] derived an equivalent mass matrix of a beam in the ascending power of the square of the frequency. He achieved this by formulating the deformation function in power series and he then illustrated his method by numerical results utilising eight segments in his dynamic discretisation model. By contrast, Melosh and Smith [3] made effective use of frequency-dependent mass and stiffness matrices of a bar element when they investigated the free vibration behaviour of pin-jointed frames as opposed to rigid-jointed frames. Clearly their theory covered bar elements, but not beam elements. Fergusson and Pilkey [4] on the other hand, gave theoretical formulations for the frequency-dependent mass and stiffness matrices of a structural element for the general case and they showed how these matrices can be related to the dynamic stiffness matrix. They also showed that Taylor series expansion of a given order can be used to truncate the frequency dependent shape function leading to the frequency-dependent mass and stiffness matrices of the structural element and yet, sufficiently accurate results can be achieved. However, they did not demonstrate the application of their theory by numerical results. Paz and Dung [5] extended Przemieniecki's work [1] by including the effect of an axial force so that both free vibration and buckling analysis of columns can be carried out. However, their investigation was entirely theoretical. They provided the expressions for the elements of the mass, stiffness and geometric matrices of beams using only first and second order terms, but without reporting any numerical results. Later Dumont and Oliveira [6] advanced the work of these earlier researchers significantly by extending the application of the frequency-dependent mass and stiffness matrices to response problems. They successfully solved the response problem of plane frames when subjected to arbitrary dynamic loads at some chosen nodes. However, as was the case with previous investigators, they also resorted to power series expansion of the frequency-dependent mass and stiffness matrices of beam elements. Thus, all these attempts made so far had some form of truncation error or other. Clearly, these investigations did not produce exact explicit expressions for the individual terms of the frequency dependent mass, elastic, and geometric stiffness matrices of a beam element. However, an exception to this trend occurred recently when

E-mail address: j.r.banerjee@city.ac.uk.

https://doi.org/10.1016/j.compstruc.2023.107235
Received 25 August 2023; Accepted 10 November 2023
Available online 9 December 2023

Banerjee [7] derived explicit exact algebraic expressions for the elements of the frequency-dependent mass and stiffness matrices of a Bernoulli-Euler beam by using symbolic computation quite rigorously. The frequency-dependent mass and stiffness expressions in Banerjee's work [7] included all the terms of the infinite series implicitly, and thus avoided any possible truncation error that was inevitably present in earlier works. However, the theory developed by Banerjee [7], significant though it was, did not include the effect of an important parameter which is that of an axial load that may be carried by the beam. It is well known that the effect of an axial load in a beam can be significant when predicting its vibration characteristics. This is particularly true when the beam carries too much of a compressive load. If the compressive load in a beam approaches its critical buckling load, the corresponding natural frequency will tend to zero, indicating a duality between the buckling and free vibration problems in the sense that buckling can be interpreted as free vibration at zero frequency. Obviously, the earlier theory developed by Banerjee [7] cannot be applied to an axially loaded beam and therefore, this paper attempts to fill this significant gap in the literature. This undeveloped research is carried out by deriving the frequency-dependent mass, elastic, and geometric stiffness matrices of the beam using symbolic computation extensively. As expected, the presence of an axial load in a beam increases the level of complexity of the problem, particularly when deriving explicit expressions for the elements of the frequency-dependent mass, elastic, and geometric stiffness matrices. The difficulty principally arises because of the lengthy algebraic expressions that are inevitably expected to appear in the derivation, which may become unwieldy and unmanageable. To circumvent this difficulty, symbolic computation which has now reached an advanced stage in its development, has been extensively used in this paper. This research might have been impossible without the symbolic computation tool. At this juncture, a brief review of the application of symbolic computation in structural engineering research is necessary.

Sathyamoorthy and Sirigiri [8] analysed box beam structures using symbolic computation techniques. Essentially, they manipulated the energy method and carried out various mathematical operations algebraically such as differentiation, integration, and matrix inversion to generate the force–displacement relationship of the box beam. The investigation is particularly relevant in determining the stiffness properties of aircraft wings for which the principal load carrying structural member is the torsion box [8]. Beltzer [9] demonstrated that considerable benefits can be achieved by applying symbolic computation when analysing engineering structures. He showed that programming with symbolic manipulation code provides additional insights into both qualitative and quantitative aspects of engineering analysis with great reliability. Pavlovic [10] published a survey paper in which he reviewed the past applications of symbolic computation in structural engineering and mechanics. He highlighted potential possibilities of symbolic computing that lie ahead. Following these advancements in symbolic computing, the author of this paper applied symbolic computation in his research on numerous occasions. For instance, he applied symbolic computation to carry out flutter analysis of aircraft wings [11], modal analysis of whole aircraft configuration [12] and free vibration analysis of axially loaded composite beams [13]. A significant piece of research by him and his colleagues in this respect, was the application of symbolic computation in Hamiltonian mechanics [14] to generate the governing differential equations of motion of complex dynamical systems. They automated the entire procedure of the variational method of Hamilton's principle by symbolic computation which necessitated integration by parts algebraically to arrive at the governing differential equations of motion. Clearly such an approach is efficient, elegant, and importantly, less error prone.

The resulting frequency-dependent mass, elastic and geometric stiffness matrices of a beam developed in this paper are related to its dynamic stiffness matrix (DSM) which is finally applied through the implementation of the Wittrick-Williams algorithm [15] as solution technique to compute the natural frequencies of axially loaded beams and frameworks. The DSM was pioneered by Kolousek [16], which is essentially an exact method with many advantages over the conventional finite element method (FEM) when carrying out free vibration analysis of structures. This is well known and well-documented in the literature, but interested readers are referred to some selective papers [17–22] which demonstrate the superiority of DSM over FEM. For instance, one single structural element can be used in DSM to determine any number of its natural frequencies to any desired accuracy, which of course, is impossible in FEM. However, it should be recognised that FEM is without doubt a universal tool in structural analysis and design, which is capable of handling complex geometries and boundaries. Although FEM is an approximate and basically a numerical method, it is sufficiently general and has applications in many other fields, particularly being effective in solving multi-physics problems. FEM has been successfully applied to investigate beam vibration problems over many years, see for example [23,24]. It is also evident from recently published literature that investigators have benefitted enormously from FEM when developing advanced beam theories [25–28]. There are some excellent texts on FEM [29,30].

The fundamental aspects and materials of this paper are organised as follows. Following this section on Introduction, Section 2 focuses on the derivation of shape functions for an axially loaded Bernoulli-Euler beam which is followed by Sections 3, 4 and 5 which describe in detail the developments of the frequency-dependent mass, elastic and geometric stiffness matrices of the beam, respectively. The materials presented in Sections 2, 3, 4 and 5 were greatly dependent on symbolic computation which was carried out by REDUCE [31,32]. It should be noted that frequency-dependent mass and stiffness matrices of a bar, undergoing axial deformation, are readily available in the literature [1,7] for which no elaboration is needed, but they are needed to investigate the free vibration behaviour of frameworks. Section 6 primarily deals with the application aspects of the theory described in Sections 2-5. Also in Section 6, the importance of incorporating the frequency-dependent axial mass and stiffness matrices of a beam already available in the literature [1,7] into the current theory is emphasised so that free vibration analysis of frameworks can be carried out. The section summarises briefly the equivalency between the frequency-dependent mass, elastic and geometric stiffness matrices and the dynamic stiffness matrix and explains the salient features of the Wittrick-Williams algorithm [15] as solution technique and how it can be applied to determine the natural frequencies. Section 7 discusses numerical results for four illustrative examples and some of the results are validated against published results and finite element analysis. The findings of the research are concluded in Section 8.

2. Frequency-dependent exact shape functions for an axially loaded beam

The first step to develop the frequency-dependent mass, elastic and geometric stiffness matrices of an axially loaded beam is to derive its frequency-dependent shape functions which relate the bending displacement and bending rotation within the beam to its nodal displacements when the beam is undergoing free natural vibration. Fig. 1 shows the coordinate system and notations for an axially loaded Bernoulli-Euler beam with bending rigidity EI, mass per unit length ρA where ρ is the density of material and A is the area of cross-section, and L is the length of the beam. Note that node 1 of the beam is located at the origin O and node 2 is at the other end at a distance L from the origin, as

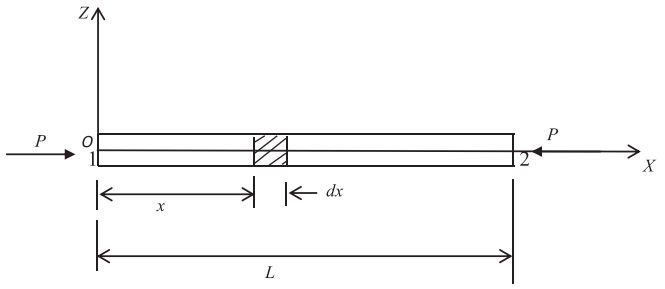

Fig. 1. Coordinate system and notation for an axially loaded Bernoulli-Euler beam.

shown in Fig. 1. A compressive axial load P as shown in the figure, is assumed to be positive, acting through the centroid of the cross-section, but P can be negative so that tension is included in the theory.

The kinetic energy (T) and potential energy (V) of the beam in the usual notation can be expressed as

$$T = \frac{1}{2}\int_0^L \rho A \dot{w}^2 dx; \quad V = \frac{1}{2}\int_0^L EI(w'')^2 dx - \frac{1}{2}\int_0^L P(w')^2 dx \tag{1}$$

where $w(x, t)$ is the bending or transverse deflection in the Z-direction and a prime and an over-dot represent differentiation with respect to the length coordinate x and time t, respectively.

Hamilton's principle states

$$\delta \int_{t_1}^{t_2} (T - V) dt = 0 \tag{2}$$

where t_1 and t_2 are the time interval in the dynamic trajectory, and δ is the usual variational operator.

The governing differential equation of motion for the axially loaded beam in free vibration can now be derived by substituting the kinetic energy (T) and the potential energy (V) expressions given by Eq. (1) into Eq. (2), and then using the δ operator and integrating by parts, and finally collecting terms. In an earlier publication, the entire procedure to generate the governing differential equations of motion and natural boundary conditions for bar or beam type structures was automated by Banerjee et al [14] through the application of symbolic computation. In this way, the governing differential equation of the axially loaded Bernoulli-Euler beam in free vibration is obtained as

$$EIw'''' + Pw'' + \rho A \ddot{w} = 0 \tag{3}$$

Assuming harmonic oscillation so that $w(x, t) = We^{i\omega t}$ where W is the amplitude of bending or flexural vibration, ω is the circular or angular frequency and $i = \sqrt{-1}$, the above partial differential equation can be converted into the following ordinary differential equation.

$$(D^4 + p^2 D^2 - b^2)W = 0 \tag{4}$$

where

$$p^2 = \frac{PL^2}{EI}; b^2 = \frac{\rho A \omega^2 L^4}{EI}; D = \frac{d}{d\xi}; \xi = \frac{x}{L} \tag{5}$$

The solution of the above governing differential equation, i.e., Eq. (4) for the amplitudes of bending displacement $W(x)$ and bending rotation

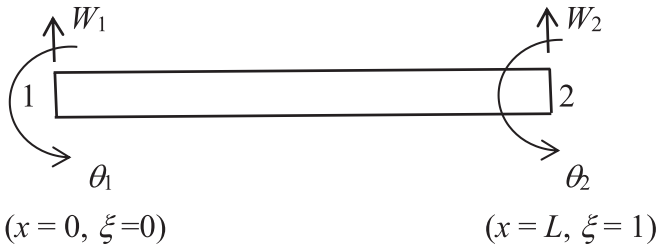

Fig. 2. End conditions for the displacements of a beam in flexural motion.

$\theta(\xi) = \frac{1}{L}W'(\xi)$ can be obtained as

$$W(\xi) = A_1\cosh\alpha\xi + A_2\sinh\alpha\xi + A_3\cos\beta\xi + A_4\sin\beta\xi \tag{6}$$

$$\theta(\xi) = \frac{1}{L}(A_1\alpha\sinh\alpha\xi + A_2\alpha\cosh\alpha\xi - A_3\beta\sin\beta\xi + A_4\beta\cos\beta\xi) \tag{7}$$

where

$$\alpha^2 = \frac{1}{2}\left(-p^2 + \sqrt{p^4 + 4b^2}\right); \quad \beta^2 = \frac{1}{2}\left(p^2 + \sqrt{p^4 + 4b^2}\right) \tag{8}$$

Referring to Fig. 2, the end conditions (or boundary conditions) for W and θ at nodes 1 and 2 can now be applied to Eqs. (6) and (7) to eliminate the constants A_1- A_4 and then formulate the shape functions.

The end conditions are:

$$\text{At node 1 } (x = 0, \text{ i.e., } \xi = 0),\ W = W_1 \text{ and } \theta = \theta_1 \tag{9}$$

$$\text{At node 2 } (x = L, \text{ i.e., } \xi = 1),\ W = W_2 \text{ and } \theta = \theta_2 \tag{10}$$

Substituting Eqs. (9) and (10) into Eqs. (6) and (7) gives the following matrix relationship

$$\begin{bmatrix} W_1 \\ \theta_1 \\ W_2 \\ \theta_2 \end{bmatrix} = \begin{bmatrix} 1 & 0 & 1 & 0 \\ 0 & \alpha/L & 0 & \beta/L \\ C_{h\alpha} & S_{h\alpha} & C_\beta & S_\beta \\ \alpha S_{h\alpha}/L & \alpha C_{h\alpha}/L & -\beta S_\beta/L & \beta C_\beta/L \end{bmatrix} \begin{bmatrix} A_1 \\ A_2 \\ A_3 \\ A_4 \end{bmatrix} \tag{11}$$

or

$$\begin{bmatrix} A_1 \\ A_2 \\ A_3 \\ A_4 \end{bmatrix} = \begin{bmatrix} 1 & 0 & 1 & 0 \\ 0 & \alpha/L & 0 & \beta/L \\ C_{h\alpha} & S_{h\alpha} & C_\beta & S_\beta \\ \alpha S_{h\alpha}/L & \alpha C_{h\alpha}/L & -\beta S_\beta/L & \beta C_\beta/L \end{bmatrix}^{-1} \begin{bmatrix} W_1 \\ \theta_1 \\ W_2 \\ \theta_2 \end{bmatrix} \tag{12}$$

where

$$C_{h\alpha} = \cosh\alpha; S_{h\alpha} = \sinh\alpha; C_\beta = \cos\beta; S_\beta = \sin\beta \tag{13}$$

Now, Eq. (6) can be written in matrix form as

$$[W(\xi)] = [\cosh\alpha\xi \quad \sinh\alpha\xi \quad \cos\beta\xi \quad \sin\beta\xi\ ] \begin{bmatrix} A_1 \\ A_2 \\ A_3 \\ A_4 \end{bmatrix} \tag{14}$$

Substituting Eq. (12) into Eq. (14) gives

$$[W(\xi)] = [\cosh\alpha\xi \quad \sinh\alpha\xi \quad \cos\beta\xi \quad \sin\beta\xi\ ] \begin{bmatrix} 1 & 0 & 1 & 0 \\ 0 & \alpha/L & 0 & \beta/L \\ C_{h\alpha} & S_{h\alpha} & C_{\beta} & S_{\beta} \\ \alpha S_{h\alpha}/L & \alpha C_{h\alpha}/L & -\beta S_{\beta}/L & \beta C_{\beta}/L \end{bmatrix}^{-1} \begin{bmatrix} W_1 \\ \theta_1 \\ W_2 \\ \theta_2 \end{bmatrix} \tag{15}$$

or

$$[W(\xi)] = [N_1 \quad N_2 \quad N_3 \quad N_4\ ] \begin{bmatrix} W_1 \\ \theta_1 \\ W_2 \\ \theta_2 \end{bmatrix} \tag{16}$$

i.e.,

$$\boldsymbol{\delta} = \mathbf{N}\boldsymbol{\delta}_{\mathbf{N}} \tag{17}$$

where $\mathbf{N}$ is the shape function comprising N_1, N_2, N_3 and N_4 terms relating displacement $W(\xi)$ within the element, i.e., $\boldsymbol{\delta}$ to the nodal displacements, i.e., $\boldsymbol{\delta}_{\mathbf{N}}$ which are W_1, θ_1 (at node 1) and W_2, θ_2 (at node 2).

The task of generating the shape function in short, compact, and concise algebraic form by performing the matrix inversion and multiplication steps of Eq. (15) was somehow challenging. This undertaking was greatly assisted by the application of symbolic computation [31,32]. Thus, the explicit expressions for the shape functions N_1, N_2, N_3 and N_4 were derived by extensive use of the symbolic computation package REDUCE [32]. These are given by

$$N_1 = -\mu_1\beta\cosh\alpha\xi + \mu_3\beta\sinh\alpha\xi + \mu_2\alpha\cos\beta\xi - \mu_3\alpha\sin\beta\xi \tag{18}$$

$$N_2 = L(-\mu_4\cosh\alpha\xi + \mu_2\sinh\alpha\xi + \mu_4\cos\beta\xi - \mu_1\sin\beta\xi) \tag{19}$$

$$N_3 = -\mu_7\alpha\beta\cosh\alpha\xi - \mu_5\beta\sinh\alpha\xi + \mu_7\alpha\beta\cos\beta\xi + \mu_5\alpha\sin\beta\xi \tag{20}$$

$$N_4 = L(\mu_6\cosh\alpha\xi - \mu_7\beta\sinh\alpha\xi - \mu_6\cos\beta\xi + \mu_7\alpha\sin\beta\xi) \tag{21}$$

where

$$\mu_1 = \left(\alpha C_{h\alpha}C_{\beta} + \beta S_{h\alpha}S_{\beta} - \alpha\right)/\Delta \tag{22}$$

$$\mu_2 = \left(\alpha S_{h\alpha}S_{\beta} - \beta C_{h\alpha}C_{\beta} + \beta\right)/\Delta \tag{23}$$

$$\mu_3 = \left(\alpha S_{h\alpha}C_{\beta} + \beta C_{h\alpha}S_{\beta}\right)/\Delta \tag{24}$$

$$\mu_4 = \left(\alpha C_{h\alpha}S_{\beta} - \beta S_{h\alpha}C_{\beta}\right)/\Delta \tag{25}$$

$$\mu_5 = \left(\alpha S_{h\alpha} + \beta S_{\beta}\right)/\Delta \tag{26}$$

$$\mu_6 = \left(\alpha S_{\beta} - \beta S_{h\alpha}\right)/\Delta \tag{27}$$

$$\mu_7 = \left(C_{\beta} - C_{h\alpha}\right)/\Delta \tag{28}$$

with

$$\Delta = \left(\alpha^2 - \beta^2\right)S_{h\alpha}S_{\beta} + 2\alpha\beta(1 - C_{h\alpha}C_{\beta}) \tag{29}$$

The frequency-dependent mass ($\mathbf{m}$), elastic ($\mathbf{k_E}$) and geometric ($\mathbf{k_G}$) stiffness matrices can now be formulated as follows.

3. Frequency-dependent mass matrix

The frequency-dependent mass ($\mathbf{m}$) matrix can now be formulated as follows [7].

$$\mathbf{m} = \int_V \rho\mathbf{N}^T\mathbf{N}dv = \rho AL\int_0^1 \begin{bmatrix} N_1 \\ N_2 \\ N_3 \\ N_4 \end{bmatrix} [N_1 \quad N_2 \quad N_3 \quad N_4\ ]d\xi = \begin{bmatrix} m_{11} & m_{12} & m_{13} & m_{14} \\ m_{21} & m_{22} & m_{23} & m_{24} \\ m_{31} & m_{32} & m_{33} & m_{34} \\ m_{41} & m_{42} & m_{43} & m_{44} \end{bmatrix} \tag{30}$$

Substituting the expressions for the shape functions N_1, N_2, N_3 and N_4 from Eqs. (18)–(21) into Eq. (30) and then carrying out the integration algebraically with the help of symbolic computation [32] made it possible after expending some concerted efforts to generate explicit expressions for each of the elements of the frequency-dependent mass matrix as follows.

$$\left.\begin{aligned} m_{11} = m_{33} &= \rho AL\Phi_1 \\ m_{12} = m_{21} = -m_{34} = -m_{43} &= \rho AL^2\Phi_2 \\ m_{13} = m_{31} &= \rho AL\Phi_3 \\ m_{14} = m_{41} = -m_{23} = -m_{32} &= \rho AL^2\Phi_4 \\ m_{22} = m_{44} &= \rho AL^3\Phi_5 \\ m_{24} = m_{42} &= \rho AL^3\Phi_6 \end{aligned}\right\} \tag{31}$$

where

$$\Phi_1 = -\alpha^2\mu_5\mu_7C_{\beta}^2 + \left(\frac{\alpha^2\lambda_2}{2\beta}\right)C_{\beta}S_{\beta} - \left(\frac{2\alpha\beta^2\gamma_2}{\alpha_1}\right)S_{h\alpha}C_{\beta} + \beta^2\mu_5\mu_7C_{h\alpha}^2 - \left(\frac{2\alpha^2\beta\lambda_1}{\alpha_1}\right)C_{h\alpha}S_{\beta} + \left(\frac{\beta^2\gamma_1}{2\alpha}\right)C_{h\alpha}S_{h\alpha} - 2\alpha\beta\mu_5\mu_7S_{h\alpha}S_{\beta} + \Lambda_1 \tag{32}$$

$$\Phi_2 = \left(\frac{\alpha\delta_2}{2\beta}\right)C_{\beta}^2 + \frac{\gamma_5}{\alpha_1}C_{h\alpha}C_{\beta} - \frac{\alpha\delta_5}{2\beta}C_{\beta}S_{\beta} - \frac{\beta_2\beta_6}{\alpha_1}S_{h\alpha}C_{\beta} - \frac{\beta\delta_2}{2\alpha}C_{h\alpha}^2 - \frac{\beta_2\beta_3}{\alpha_1}C_{h\alpha}S_{\beta} + \frac{\beta\delta_4}{2\alpha}C_{h\alpha}S_{h\alpha} + \left(\mu_3\mu_4 + \frac{\alpha\beta\delta_1}{\alpha_1}\right)S_{h\alpha}S_{\beta} + \Lambda_2 \tag{33}$$

$$\Phi_3 = \frac{\alpha^2\zeta_6}{2\beta}C_{\beta}^2 - \frac{\alpha\beta\beta_5\mu_5}{\alpha_1}C_{h\alpha}C_{\beta} + \frac{\alpha^2\zeta_5}{2\beta}C_{\beta}S_{\beta} - \frac{\alpha\beta}{\alpha_1}(\alpha\beta_2\mu_7 + 2\beta\mu_3\mu_5)S_{h\alpha}C_{\beta} - \frac{\beta^2\xi_3}{2\alpha}C_{h\alpha}^2 + \frac{\alpha\beta}{\alpha_1}(2\alpha\mu_3\mu_5 - \beta\beta_2\mu_7)C_{h\alpha}S_{\beta} + \frac{\beta^2\xi_2}{2\alpha}C_{h\alpha}S_{h\alpha} + \frac{\alpha\beta}{\alpha_1}(\alpha_1\mu_3\mu_7 - \beta_1\mu_5)S_{h\alpha}S_{\beta} + \Lambda_3 \tag{34}$$

$$\Phi_4 = -\frac{\alpha\xi_1}{2\beta}C_{\beta}^2 - \frac{\alpha\beta\beta_5\mu_7}{\alpha_1}C_{h\alpha}C_{\beta} + \frac{\alpha\xi_4}{2\beta}C_{\beta}S_{\beta} + \frac{\alpha}{\alpha_1}\left(\beta_2\mu_6 - 2\beta^2\mu_3\mu_7\right)S_{h\alpha}C_{\beta} + \frac{\beta\zeta_3}{2\alpha}C_{h\alpha}^2 + \frac{\beta}{\alpha_1}\left(\beta_2\mu_6 + 2\alpha^2\mu_3\mu_7\right)C_{h\alpha}S_{\beta} - \frac{\beta\zeta_2}{2\alpha}C_{h\alpha}S_{h\alpha} - \frac{1}{\alpha_1}(\alpha\beta\beta_1\mu_7 + \alpha_1\mu_3\mu_6)S_{h\alpha}S_{\beta} + \Lambda_4 \tag{35}$$

$$\Phi_5 = \frac{\alpha\mu_6\mu_7}{\beta}C_\beta^2 - \frac{\gamma_4}{2\beta}C_\beta S_\beta + \frac{2\alpha\lambda_4}{\alpha_1}S_{h\alpha}C_\beta - \frac{\beta\mu_6\mu_7}{\alpha}C_{h\alpha}^2 - \frac{2\beta\gamma_3}{\alpha_1}C_{h\alpha}S_\beta + \frac{\lambda_3}{2\alpha}C_{h\alpha}S_{h\alpha} + 2\mu_6\mu_7 S_{h\alpha}S_\beta + \Lambda_5 \tag{36}$$

$$\Phi_6 = -\frac{\xi_6}{2\beta}C_\beta^2 - \frac{\beta_5\mu_6}{\alpha_1}C_{h\alpha}C_\beta + \frac{\xi_5}{2\beta}C_\beta S_\beta + \frac{1}{\alpha_1}(2\alpha\mu_4\mu_6 - \beta\beta_2\mu_7)S_{h\alpha}C_\beta + \frac{\zeta_4}{2\alpha}C_{h\alpha}^2 + \frac{1}{\alpha_1}(\alpha\beta_2\mu_7 + 2\beta\mu_4\mu_6)C_{h\alpha}S_\beta - \frac{\zeta_1}{2\alpha}C_{h\alpha}S_{h\alpha} - \frac{1}{\alpha_1}(\alpha_1\mu_4\mu_7 + \beta_1\mu_6)S_{h\alpha}S_\beta + \Lambda_6 \tag{37}$$

where

$$\left.\begin{aligned}\alpha_1 &= \alpha^2 + \beta^2;\quad \alpha_2 = \alpha^2 - \beta^2;\quad \alpha_3 = \alpha^4 + \beta^4\\ \alpha_4 &= \alpha^4 - \beta^4;\quad \alpha_5 = 3\alpha^2 + \beta^2;\quad \alpha_6 = \alpha^2 + 3\beta^2\end{aligned}\right\} \tag{38}$$

$$\left.\begin{aligned}\beta_1 &= \alpha\mu_1 + \beta\mu_2;\ \beta_2 = \alpha\mu_2 + \beta\mu_1;\ \beta_3 = \alpha\mu_3 + \beta\mu_4\\ \beta_4 &= \alpha\mu_1 - \beta\mu_2;\ \beta_5 = \alpha\mu_2 - \beta\mu_1;\ \beta_6 = \alpha\mu_4 - \beta\mu_3\end{aligned}\right\} \tag{39}$$

$$\left.\begin{aligned}\gamma_1 &= \alpha^2\mu_7^2 + \mu_5^2;\ \gamma_2 = \alpha^2\mu_7^2 - \mu_5^2;\ \gamma_3 = \alpha^2\mu_7^2 + \mu_6^2\\ \gamma_4 &= \alpha^2\mu_7^2 - \mu_6^2;\ \gamma_5 = \alpha^2\mu_2^2 - \beta^2\mu_1^2;\ \gamma_6 = \alpha^2\mu_2 - \beta^2\mu_1\end{aligned}\right\} \tag{40}$$

$$\lambda_1 = \beta^2\mu_7^2 + \mu_5^2; \lambda_2 = \beta^2\mu_7^2 - \mu_5^2; \lambda_3 = \beta^2\mu_7^2 + \mu_6^2; \lambda_4 = \beta^2\mu_7^2 - \mu_6^2 \tag{41}$$

$$\left.\begin{aligned}\delta_1 &= \mu_1^2 + \mu_2^2; \delta_2 = \mu_1\mu_2 + \mu_3\mu_4; \delta_3 = \mu_1\mu_3 + \mu_2\mu_4\\ \delta_4 &= \mu_1\mu_4 + \mu_2\mu_3; \delta_5 = \mu_1\mu_3 - \mu_2\mu_4; \delta_6 = \mu_1\mu_4 - \mu_2\mu_3\end{aligned}\right\} \tag{42}$$

$$\left.\begin{aligned}\xi_1 &= \alpha\mu_2\mu_7 + \mu_3\mu_6;\ \xi_2 = \alpha\mu_1\mu_7 - \mu_3\mu_5;\ \xi_3 = \alpha\mu_3\mu_7 - \mu_1\mu_5\\ \xi_4 &= \alpha\mu_3\mu_7 - \mu_2\mu_6;\ \xi_5 = \alpha\mu_1\mu_7 - \mu_4\mu_6;\ \xi_6 = \alpha\mu_4\mu_7 + \mu_1\mu_6\end{aligned}\right\} \tag{43}$$

$$\left.\begin{aligned}\zeta_1 &= \beta\mu_2\mu_7 + \mu_4\mu_6; \zeta_2 = \beta\mu_3\mu_7 + \mu_1\mu_6; \zeta_3 = \beta\mu_1\mu_7 + \mu_3\mu_6\\ \zeta_4 &= \beta\mu_4\mu_7 + \mu_2\mu_6; \zeta_5 = \beta\mu_2\mu_7 + \mu_3\mu_5; \zeta_6 = \beta\mu_3\mu_7 - \mu_2\mu_5;\ \zeta_7 = \beta\mu_2\mu_7 - \mu_4\mu_6\end{aligned}\right\} \tag{44}$$

and

$$\Lambda_1 = \alpha^2\beta^2\mu_7^2 + \frac{\alpha_2\mu_5}{2}(\mu_5 + 2\mu_7) \tag{45}$$

$$\Lambda_2 = \frac{1}{2\alpha\beta\alpha_1}\left(\alpha\alpha_1\beta^2\delta_6 + \alpha^2\alpha_1\beta\delta_3 - \alpha_1\alpha_2\delta_2 - 2\alpha\beta\gamma_5\right) \tag{46}$$

$$\Lambda_3 = \frac{1}{2\alpha\alpha_1\beta}\left(\alpha^3\alpha_6\mu_2\mu_5 + \alpha^2\alpha_1\beta^2\beta_2\mu_7 - \alpha\alpha_1\alpha_2\beta\mu_3\mu_5 - \alpha\alpha_1\alpha_2\beta\mu_3\mu_7 - \alpha_5\beta^3\mu_1\mu_5\right) \tag{47}$$

$$\Lambda_4 = \frac{1}{2\alpha\beta\alpha_1}\left(\alpha^3\alpha_6\mu_2\mu_7 - \alpha\alpha_1\alpha_2\beta\mu_3\mu_7 - \alpha^2\alpha_1\beta\mu_2\mu_6 + \alpha_1\alpha_2\alpha_3\mu_6 - \alpha\alpha_1\beta^2\mu_1\mu_6 - \alpha_5\beta^3\mu_1\mu_7\right) \tag{48}$$

$$\Lambda_5 = \mu_6^2 + \frac{\alpha_2\mu_7(\alpha\beta\mu_7 - 2\mu_6)}{2\alpha\beta} \tag{49}$$

$$\Lambda_6 = \frac{1}{2\alpha\beta\alpha_1}\left(-\alpha\alpha_1\beta\beta_4\mu_7 + \alpha_1\alpha_2\mu_4\mu_7 + \alpha_2\beta_1\mu_6 - 2\alpha\alpha_1\beta\mu_4\mu_6\right) \tag{50}$$

4. Frequency-dependent elastic stiffness matrix

The frequency-dependent elastic stiffness matrix of an axially loaded beam follows from the procedure given by [7]

$$\mathbf{k}_\mathrm{E}(\omega) = \int_V \mathbf{B}^\mathrm{T}\mathbf{D}\mathbf{B}dv = EI\int_0^L \mathbf{B}^\mathrm{T}\mathbf{B}dx = EIL\int_0^1 \mathbf{B}^\mathrm{T}\mathbf{B}\mathrm{d}\xi \tag{51}$$

where **B** matrix relates the strains within the element to nodal displacements, and **D** matrix defines the constitutive law, i.e., the stress–strain relationship and the integration is carried out throughout the volume of the element. For a beam element the **D** matrix is effectively the Young's modulus E of the material and when the integration is carried out over the area of cross-section, the constant term EI appears outside the integration sign of Eq. (51).

The **B** matrix in terms of the shape functions N_1, N_2, N_3 and N_4 is given by [7]

$$\mathbf{B} = \frac{1}{L^2}\left[\frac{d^2N_1}{d\xi^2}\quad \frac{d^2N_2}{d\xi^2}\quad \frac{d^2N_3}{d\xi^2}\quad \frac{d^2N_4}{d\xi^2}\right] = \frac{1}{L^2}\left[N_1^{''}(\xi), N_2^{''}(\xi), N_3^{''}(\xi), N_4^{''}(\xi)\right] \tag{52}$$

Thus, the frequency-dependent elastic stiffness matrix of Eq (51) can be written as

$$\mathbf{k}_\mathrm{E} = \frac{EI}{L^3}\int_0^1 \begin{bmatrix} N_1^{''}\\ N_2^{''}\\ N_3^{''}\\ N_4^{''}\end{bmatrix}\begin{bmatrix} N_1^{''} & N_2^{''} & N_3^{''} & N_4^{''}\end{bmatrix}d\xi = \begin{bmatrix} k_{11}^E & k_{12}^E & k_{13}^E & k_{14}^E\\ k_{21}^E & k_{22}^E & k_{23}^E & k_{24}^E\\ k_{31}^E & k_{32}^E & k_{33}^E & k_{34}^E\\ k_{41}^E & k_{42}^E & k_{43}^E & k_{44}^E\end{bmatrix} \tag{53}$$

By extensive algebraic manipulation using symbolic computation [31,32], the individual elements of the frequency dependent elastic stiffness matrices $\mathbf{k}_\mathbf{E}$ were generated in explicit algebraic form. The final expressions for the elements are given below in concise form.

$$\left.\begin{aligned} k_{11}^E(\omega) = k_{33}^E(\omega) &= \left(\frac{EI}{L^3}\right)\Psi_1\\ k_{12}^E(\omega) = k_{21}^E(\omega) = -k_{34}^E(\omega) = -k_{43}^E(\omega) &= \left(\frac{EI}{L^3}\right)\Psi_2 L\\ k_{13}^E(\omega) = k_{31}^E(\omega) &= \left(\frac{EI}{L^3}\right)\Psi_3\\ k_{14}^E(\omega) = k_{41}^E(\omega) = -k_{23}^E(\omega) = -k_{32}^E(\omega) &= \left(\frac{EI}{L^3}\right)\Psi_4 L\\ k_{22}^E(\omega) = k_{44}^E(\omega) &= \left(\frac{EI}{L^3}\right)\Psi_5 L^2\\ k_{24}^E(\omega) = k_{42}^E(\omega) &= \left(\frac{EI}{L^3}\right)\Psi_6 L^2\end{aligned}\right\} \tag{54}$$

where

$$\Psi_1 = -\alpha^2\beta^4\mu_5\mu_7 C_\beta^2 + \frac{\alpha^2\beta^3\lambda_2}{2}C_\beta S_\beta + \frac{2\alpha^3\beta^4\gamma_2}{\alpha_1}S_{h\alpha}C_\beta + \alpha^4\beta^2\mu_5\mu_7 C_{h\alpha}^2 + \frac{2\alpha^4\beta^3\lambda_1}{\alpha_1}C_{h\alpha}S_\beta + \frac{\alpha^3\beta^2\gamma_1}{2}C_{h\alpha}S_{h\alpha} + 2\alpha^3\beta^3\mu_5\mu_7 S_{h\alpha}S_\beta + \Gamma_1 \tag{55}$$

$$\Psi_2 = \frac{\alpha\beta^3\delta_2}{2}C_\beta^2 - \frac{\alpha^2\beta^2\gamma_5}{\alpha_1}C_{h\alpha}C_\beta - \frac{\alpha\beta^3\delta_5}{2}C_\beta S_\beta + \frac{\alpha^2\beta^2\beta_2\beta_6}{\alpha_1}S_{h\alpha}C_\beta - \frac{\alpha^3\beta\delta_2}{2}C_{h\alpha}^2 + \frac{\alpha^2\beta^2\beta_2\beta_3}{\alpha_1}C_{h\alpha}S_\beta + \frac{\alpha^3\beta\delta_4}{2}C_{h\alpha}S_{h\alpha} - \frac{\alpha^2\beta^2}{\alpha_1}(\alpha_1\mu_3\mu_4 + \alpha\beta\delta_1)S_{h\alpha}S_\beta + \Gamma_2 \tag{56}$$

$$\Psi_3 = \frac{\alpha^2\beta^3\zeta_6}{2}C_\beta^2 + \frac{\alpha^3\beta^3\beta_5\mu_5}{\alpha_1}C_{h\alpha}C_\beta + \frac{\alpha^2\beta^3\zeta_5}{2}C_\beta S_\beta + \frac{\alpha^3\beta^3}{\alpha_1}(\alpha\beta_2\mu_7 + 2\beta\mu_3\mu_5)S_{h\alpha}C_\beta - \frac{\alpha^3\beta^2\xi_3}{2}C_{h\alpha}^2 + \frac{\alpha^3\beta^3}{\alpha_1}(\beta\beta_2\mu_7 - 2\alpha\mu_3\mu_5)C_{h\alpha}S_\beta + \frac{\alpha^3\beta^2\xi_2}{2}C_{h\alpha}S_{h\alpha} - \frac{\alpha^3\beta^3}{\alpha_1}(\alpha_1\mu_3\mu_7 - \beta_1\mu_5)S_{h\alpha}S_\beta + \Gamma_3 \tag{57}$$

$$\Psi_4 = -\frac{\alpha\beta^3\xi_1}{2}C_\beta^2 + \frac{\alpha^3\beta^3\beta_5\mu_7}{\alpha_1}C_{h\alpha}C_\beta + \frac{\alpha\beta^3\xi_4}{2}C_\beta S_\beta - \frac{\alpha^3\beta^2}{\alpha_1}(\beta_2\mu_6 - 2\beta^2\mu_3\mu_7)S_{h\alpha}C_\beta + \frac{\alpha^3\beta\zeta_3}{2}C_{h\alpha}^2 - \frac{\alpha^2\beta^3}{\alpha_1}(\beta_2\mu_6 + 2\alpha^2\mu_3\mu_7)C_{h\alpha}S_\beta - \frac{\alpha^3\beta\zeta_2}{2}C_{h\alpha}S_{h\alpha} + \frac{\alpha^2\beta^2}{\alpha_1}(\alpha\beta\beta_1\mu_7 + \alpha_1\mu_3\mu_6)S_{h\alpha}S_\beta + \Gamma_4 \tag{58}$$

$$\Psi_5 = \alpha\beta^3\mu_6\mu_7C_\beta^2 - \frac{\beta^3\gamma_4}{2}C_\beta S_\beta - \frac{2\alpha^3\beta^2\lambda_4}{\alpha_1}S_{h\alpha}C_\beta - \alpha^3\beta\mu_6\mu_7C_{h\alpha}^2 + \frac{2\alpha^2\beta^3\gamma_3}{\alpha_1}C_{h\alpha}S_\beta + \frac{\alpha^3\lambda_3}{2}C_{h\alpha}S_{h\alpha} - 2\alpha^2\beta^2\mu_6\mu_7S_{h\alpha}S_\beta + \Gamma_5 \tag{59}$$

$$\Psi_6 = -\frac{\beta^3\xi_6}{2}C_\beta^2 + \frac{\alpha^2\beta^2\beta_5\mu_6}{\alpha_1}C_{h\alpha}C_\beta + \frac{\beta^3\xi_5}{2}C_\beta S_\beta + \frac{\alpha^2\beta^2}{\alpha_1}(\beta\beta_2\mu_7 - 2\alpha\mu_4\mu_6)S_{h\alpha}C_\beta + \frac{\alpha^3\zeta_4}{2}C_{h\alpha}^2 - \frac{\alpha^2\beta^2}{\alpha_1}(\alpha\beta_2\mu_7 + 2\beta\mu_4\mu_6)C_{h\alpha}S_\beta - \frac{\alpha^3\zeta_1}{2}C_{h\alpha}S_{h\alpha} + \frac{\alpha^2\beta^2}{\alpha_1}(\alpha_1\mu_4\mu_7 + \beta_1\mu_6)S_{h\alpha}S_\beta + \Gamma_6 \tag{60}$$

with

$$\Gamma_1 = \frac{\alpha^2\beta^2}{2}\left(\alpha_3\mu_7^2 - \alpha_2\mu_5^2 - 2\alpha_2\mu_5\mu_7\right) \tag{61}$$

$$\Gamma_2 = \frac{\alpha\beta}{2\alpha_1}\left(\alpha^3\alpha_1\delta_6 + \alpha_1\alpha_2\delta_2 + 2\alpha\beta\gamma_5 + \alpha_1\beta^3\delta_3\right) \tag{62}$$

$$\Gamma_3 = \frac{\alpha^2\beta^2}{2\alpha_1}\left\{\alpha_1\mu_7\left(\alpha^3\mu_1 + \beta^3\mu_2\right) + \alpha_1\alpha_2\mu_3(\mu_5 + \mu_7) - \alpha_2\beta_1\mu_5\right\} \tag{63}$$

$$\Gamma_4 = \frac{\alpha\beta}{2\alpha_1}\left\{-\alpha_1\mu_6\left(\alpha^3\mu_1 + \beta^3\mu_2\right) - \alpha\alpha_2\beta\beta_1\mu_7 + \alpha_1\alpha_2(\alpha\beta\mu_3\mu_7 - \mu_3\mu_6)\right\} \tag{64}$$

$$\Gamma_5 = \frac{1}{2}\left(\alpha_3\mu_6^2 - \alpha^2\alpha_2\beta^2\mu_7^2 + 2\alpha\alpha_2\beta\mu_6\mu_7\right) \tag{65}$$

$$\Gamma_6 = \frac{1}{2\alpha_1}\left\{\alpha\alpha_1\beta\mu_7\left(\alpha^3\mu_2 - \beta^3\mu_1\right) - \alpha_1\mu_4\mu_6\left(\alpha^4 + \beta^4\right) - \alpha^3\alpha_6\mu_2\mu_6 + \alpha_5\beta^3\mu_1\mu_6 - \alpha\alpha_1\alpha_2\beta\mu_4\mu_7\right\} \tag{66}$$

and the rest of the terms in Eqs. (55)–(66) have already been defined by Eqs. (38)–(44) in Section 3.

5. Frequency-dependent geometric stiffness matrix

The geometric stiffness matrix of a beam of length L under the action of a compressive load P in terms of the shape functions N_1, N_2, N_3 and N_4, is given by

$$\mathbf{k}_G = -\frac{P}{L}\int_0^1 \begin{bmatrix} N_1' \\ N_2' \\ N_3' \\ N_4' \end{bmatrix}\begin{bmatrix} N_1' & N_2' & N_3' & N_4' \end{bmatrix}d\xi = \begin{bmatrix} k_{11}^G & k_{12}^G & k_{13}^G & k_{14}^G \\ k_{21}^G & k_{22}^G & k_{23}^G & k_{24}^G \\ k_{31}^G & k_{32}^G & k_{33}^G & k_{34}^G \\ k_{41}^G & k_{42}^G & k_{43}^G & k_{44}^G \end{bmatrix} \tag{67}$$

Note that the negative sign in front of Eq. (67) arises because compressive force has been taken to be positive in this paper.

Substituting the expressions for the shape functions from Eqs. (18)–(21) into Eq. (67) and performing the differentiation and integration algebraically through the application of symbolic computation [32], yielded the terms of the geometric stiffness matrix explicitly and concisely, as follows.

$$\left.\begin{aligned} k_{11}^G &= k_{33}^G = -\frac{P}{L}\Theta_1 \\ k_{12}^G(\omega) &= k_{21}^G(\omega) = -k_{34}^G(\omega) = -k_{43}^G(\omega) = -\frac{P}{L}\Theta_2 L \\ k_{13}^G(\omega) &= k_{31}^G(\omega) = -\left(\frac{P}{L}\right)\Theta_3 \\ k_{14}^G(\omega) &= k_{41}^G(\omega) = -k_{23}^G(\omega) = -k_{32}^G(\omega) = -\left(\frac{P}{L}\right)\Theta_4 L \\ k_{22}^G(\omega) &= k_{44}^G(\omega) = -\left(\frac{P}{L}\right)\Theta_5 L^2 \\ k_{24}^G(\omega) &= k_{42}^G(\omega) = -\left(\frac{P}{L}\right)\Theta_6 L^2 \end{aligned}\right\} \tag{68}$$

where

$$\Theta_1 = \alpha^2\beta^2\mu_5\mu_7C_\beta^2 - 2\alpha^2\beta^2\mu_5\mu_7C_{h\alpha}C_\beta - \frac{\alpha^2\beta\lambda_2}{2}C_\beta S_\beta - \frac{2\alpha^3\beta^2\lambda_1}{\alpha_1}S_{h\alpha}C_\beta + \alpha^2\beta^2\mu_5\mu_7C_{h\alpha}^2 + \frac{2\alpha^2\beta^3\gamma_2}{\alpha_1}C_{h\alpha}S_\beta + \frac{\alpha\beta^2\gamma_1}{2}C_{h\alpha}S_{h\alpha} + \Sigma_1 \tag{69}$$

$$\Theta_2 = -\frac{\alpha\beta\delta_2}{2}C_\beta^2 + \frac{\alpha\beta}{\alpha_1}(\alpha_1\mu_3\mu_4 + \alpha\beta\delta_1)C_{h\alpha}C_\beta + \frac{\alpha\beta\delta_5}{2}C_\beta S_\beta - \frac{\alpha\beta\beta_2\beta_3}{\alpha_1}S_{h\alpha}C_\beta - \frac{\alpha\beta\delta_2}{2}C_{h\alpha}^2 + \frac{\alpha\beta\beta_2\beta_6}{\alpha_1}C_{h\alpha}S_\beta + \frac{\alpha\beta\delta_4}{2}C_{h\alpha}S_{h\alpha} - \frac{\alpha\beta\gamma_5}{\alpha_1}S_{h\alpha}S_\beta + \Sigma_2 \tag{70}$$

$$\Theta_3 = -\frac{\alpha^2\beta\zeta_6}{2}C_\beta^2 + \frac{\alpha^2\beta^2}{\alpha_1}(\alpha_1\mu_3\mu_7 - \beta_1\mu_5)C_{h\alpha}C_\beta - \frac{\alpha^2\beta\zeta_5}{2}C_\beta S_\beta + \frac{\alpha^2\beta^2}{\alpha_1}(2\alpha\mu_3\mu_5 - \beta\beta_2\mu_7)S_{h\alpha}C_\beta - \frac{\alpha\beta^2\xi_3}{2}C_{h\alpha}^2 + \frac{\alpha^2\beta^2}{\alpha_1}(\alpha\beta_2\mu_7 + 2\beta\mu_3\mu_5)C_{h\alpha}S_\beta + \frac{\alpha\beta^2\xi_2}{2}C_{h\alpha}S_{h\alpha} + \frac{\alpha^2\beta^2\beta_5\mu_5}{\alpha_1}S_{h\alpha}S_\beta + \Sigma_3 \tag{71}$$

$$\Theta_4 = \frac{\alpha\beta\xi_1}{2}C_\beta^2 - \frac{\alpha\beta}{\alpha_1}(\alpha_1\mu_3\mu_6 + \alpha\beta\beta_1\mu_7)C_{h\alpha}C_\beta - \frac{\alpha\beta\xi_4}{2}C_\beta S_\beta + \frac{\alpha\beta^2}{\alpha_1}\left(2\alpha^2\mu_3\mu_7 + \beta_2\mu_6\right)S_{h\alpha}C_\beta + \frac{\alpha\beta\zeta_3}{2}C_{h\alpha}^2 + \frac{\alpha^2\beta}{\alpha_1}\left(2\beta^2\mu_3\mu_7 - \beta_2\mu_6\right)C_{h\alpha}S_\beta - \frac{\alpha\beta\zeta_2}{2}C_{h\alpha}S_{h\alpha} + \frac{\alpha^2\beta^2\beta_5\mu_7}{\alpha_1}S_{h\alpha}S_\beta + \Sigma_4 \tag{72}$$

$$\Theta_5 = -\alpha\beta\mu_6\mu_7 C_\beta^2 + 2\alpha\beta\mu_6\mu_7 C_{h\alpha}C_\beta + \frac{\beta\gamma_4}{2}C_\beta S_\beta - \frac{2\alpha\beta^2\gamma_3}{\alpha_1}S_{h\alpha}C_\beta - \alpha\beta\mu_6\mu_7 C_{h\alpha}^2 - \frac{2\alpha^2\beta\lambda_4}{\alpha_1}C_{h\alpha}S_\beta + \frac{\alpha\lambda_3}{2}C_{h\alpha}S_{h\alpha} + \Sigma_5 \tag{73}$$

$$\Theta_6 = \frac{\beta\xi_6}{2}C_\beta^2 - \frac{\alpha\beta}{\alpha_1}(\alpha_1\mu_4\mu_7 + \beta_1\mu_6)C_{h\alpha}C_\beta - \frac{\beta\xi_5}{2}C_\beta S_\beta + \frac{\alpha\beta}{\alpha_1}(\alpha\beta_2\mu_7 + 2\beta\mu_4\mu_6)S_{h\alpha}C_\beta + \frac{\alpha\zeta_4}{2}C_{h\alpha}^2 - \frac{\alpha\beta}{\alpha_1}(2\alpha\mu_4\mu_6 - \beta\beta_2\mu_7)C_{h\alpha}S_\beta - \frac{\alpha\zeta_1}{2}C_{h\alpha}S_{h\alpha} + \frac{\alpha\beta\beta_5\mu_6}{\alpha_1}S_{h\alpha}S_\beta + \Sigma_6 \tag{74}$$

with

$$\Sigma_1 = \frac{\alpha^2\beta^2}{2}\left(2\mu_5^2 - \alpha_2\mu_7^2\right) \tag{75}$$

$$\Sigma_2 = \frac{\alpha\beta}{2\alpha_1}(2\alpha_1\mu_1\mu_2 + \alpha_1\beta\delta_3 - \alpha\alpha_1\delta_6 - 2\alpha\beta\delta_1) \tag{76}$$

$$\Sigma_3 = -\frac{\alpha\beta}{2\alpha_1}(\alpha\alpha_1\beta\beta_4\mu_7 + \alpha_2\beta_5\mu_5 + 2\alpha\alpha_1\beta\mu_3\mu_5) \tag{77}$$

$$\Sigma_4 = \frac{\alpha\beta}{2\alpha_1}(\alpha_1\beta_4\mu_6 - \alpha_2\beta_5\mu_7 - 2\alpha\alpha_1\beta\mu_3\mu_7) \tag{78}$$

$$\Sigma_5 = \alpha^2\beta^2\mu_7^2 - \frac{\alpha_2\mu_6^2}{2} \tag{79}$$

$$\Sigma_6 = \frac{1}{2\alpha_1}(\alpha_1\alpha_2\mu_4\mu_6 - \alpha\alpha_1\beta\beta_2\mu_7 - \alpha_2\beta_5\mu_6) \tag{80}$$

and the rest of the terms in Eqs. (69)- (80) have already been defined by Eqs. (38)–(44) in Section 3.

6. Application of the frequency-dependent mass, elastic and geometric stiffness matrices

The above theory can now be applied either to an individual axially loaded beam or to a framework containing such beams when investing the free vibration characteristics. This can be achieved by utilizing the Wittrick-Williams algorithm [15] which is well-suited as a solution technique in exact free vibration analysis. However, when analysing a framework, the frequency-dependent mass and stiffness matrices in axial motion [1,7] are needed which are given in Appendix A. Therefore, by using standard coordinate transformation, the frequency dependent mass, elastic and geometric stiffness matrices of each member in a frame can be assembled, prior to the application of the Wittrick-Williams algorithm, for the subsequent determination of the natural frequencies.

It should be noted that in the limiting case when the frequency ω tends to zero, the frequency-dependent mass, elastic and geometric stiffness matrices given in Sections 3, 4 and 5, converge to the corresponding frequency-independent mass, elastic and geometric stiffness matrices of the traditional FEM. However, in the expressions for the mass, elastic and geometric stiffness elements given in Eqs. (31)–(50), Eqs. (54)–(66), and Eqs. (68)–(80), the frequency ω must not be set to exactly zero, but a small value e.g., $\omega = 10^{-5}$ rad/s can be used for practical problems so that numerical overflow or ill-conditioning can be avoided and yet the degenerate case of the frequency-independent mass, elastic and geometric stiffness matrices can be obtained. These matrices resulting from the degenerate case of the present theory by using a negligibly small frequency (ω) were checked against the frequency-independent mass, elastic and geometric stiffness matrices which are generally utilised in FEM and available in the literature [1]. When validating some results by using FEM, these matrices were used (see Appendix B).

The frequency-dependent mass, elastic and geometric stiffness matrices for an axially loaded beam $\mathbf{m}(\omega)$, $\mathbf{k_E}(\omega)$ and $\mathbf{k_G}(\omega)$ derived in Sections 3, 4 and 5 can be related to its dynamic stiffness matrix $\mathbf{k_D}(\omega)$ using the following relationship.

$$\mathbf{k_D}(\omega) = \mathbf{k_E}(\omega) + \mathbf{k_G}(\omega) - \omega^2\mathbf{m}(\omega) \tag{81}$$

Once the dynamic stiffness matrix of an axially loaded beam element is established using Eq. (81), the Wittrick-Williams algorithm as solution technique, can be applied to carry out the free vibration analysis. For the general case of a frame, the frequency-dependent mass, elastic and geometric stiffness matrices for all individual elements in the frame, should be assembled using conventional transformation technique based on the orientation of the elements, as commonly employed in FEM. Thus, the overall frequency-dependent mass, elastic and geometric stiffness matrices $\mathbf{M}(\omega)$, $\mathbf{K_E}(\omega)$ and $\mathbf{K_G}(\omega)$ and hence the overall master dynamic stiffness matrix $\mathbf{K_D}(\omega)$ of the final structure can be obtained, as follows.

$$\mathbf{K_D}(\omega) = \mathbf{K_E}(\omega) + \mathbf{K_G}(\omega) - \omega^2\mathbf{M}(\omega) \tag{82}$$

As mentioned earlier, the best way to solve the eigen-value problem represented by Eq. (82) is to apply the well-established algorithm of Wittrick and Williams [15] to determine the natural frequencies and the subsequent mode shapes of the structure. The Wittrick-Williams algorithm has widespread coverage in the literature with literally hundreds of papers published on the subject, see for example [17–20]. In many ways, the dynamic stiffness method and the Wittrick-Williams algorithm are permanently entangled with each other, as evident from the literature [17–20]. The working principle of the algorithm is essentially based on two factors which govern the solution technique. These factors known as (i) the sign-count s{$\mathbf{K_D}$} and (ii) the j_0 count, are briefly explained below.

If ω denotes the circular (or angular) frequency of a vibrating structure, then according to the Wittrick-Williams algorithm, j, the number of natural frequencies passed, as ω is increased from zero to ω^*, is given by

$$j = j_0 + s\{\boldsymbol{K_D}\} \tag{83}$$

where $\mathbf{K_D}$, the overall dynamic stiffness matrix of the final structure whose elements all depend on ω, is evaluated at $\omega = \omega^*$; s{$\mathbf{K_D}$}, the sign count, is the number of negative elements on the leading diagonal of $\mathbf{K_D^\Delta}$, $\mathbf{K_D^\Delta}$ is the upper triangular matrix obtained by applying the usual form of Gauss elimination to $\mathbf{K_D}$, and j_0 is the number of natural frequencies of the structure still lying between $\omega = 0$ and $\omega = \omega^*$ when the displacement components to which $\mathbf{K_D}$ corresponds are all zeros. (Note that the structure can still have natural frequencies when all its nodes are clamped, because exact member equations allow each individual member to displace between nodes with an infinite number of degrees of freedom, and hence an infinite number of natural frequencies between nodes.) Thus

$$j_0 = \sum j_m \tag{84}$$

where j_m is the number of natural frequencies between $\omega = 0$ and $\omega = \omega^*$ for a component member with its ends fully clamped, while the summation extends over all members of the structure. The clamped–-clamped natural frequencies of an individual member are given by the determinant of its dynamic stiffness matrix $\mathbf{K_D}(\omega)$ given by Eq. (82). Thus, with the knowledge of Eqs. (83) and (84), it is possible to ascertain how many natural frequencies of a structure lie below an arbitrarily chosen trial frequency. This simple feature of the algorithm (coupled with the fact that successive trial frequencies can be chosen to bracket a natural frequency) can be used to converge upon any required natural frequency to any desired accuracy.

7. Numerical results and discussion

The theory developed above was applied to a wide range of problems and it was ascertained that the frequency-dependent mass, elastic and geometric stiffness matrices give the same results that can be obtained by the conventional dynamic stiffness method which uses a single matrix containing the mass, elastic and geometric stiffness properties, rather than using them separately. Only selective results using some illustrative examples are presented here. The first example focuses on the free vibration behaviour of an axially loaded beam with clamped-free (C-F) pinned–pinned (P-P) and clamped–clamped (C–C) boundary conditions and under the action of both compressive and tensile loads. Deriving the frequency equation of the beam for each of the above boundary conditions, Amba-Rao [33] investigated the problem by considering only the compressive load, and his method is applicable to a single column and cannot be applied to frameworks. He presented results up to four significant figures for the fundamental natural frequency of the column in non-dimensional form for a range of compressive loads expressed as a fraction of the corresponding critical buckling load. For comparison purposes, matching results with compressive loads as well as additional results with tensile loads were computed using the present theory by utilising the frequency-dependent mass, elastic and geometric stiffness matrices and the Wittrick-Williams algorithm. The results are shown in Table 1 for representative values of axial force ratios relative to the critical buckling load. The results for the compressive loads agreed very well (up to three to four significant figures) with those reported by Amba-Rao [33] and the results for the tensile loads were checked using the well-established computer program BUNVIS-RG [34] based on the dynamic stiffness method, and complete agreement of results was found. Note that when obtaining the results for the axial force ratio $P/P_{cr} = 1$, using the present theory, the axial load P was taken to be 99.9 % of the critical buckling load P_{cr}, rather than 100 %. This was necessary to avoid any numerical overflow or ill-conditioning in the computed results. The fundamental natural frequency converged very close to zero for $P/P_{cr} = 0.999$. An illustration of the effect of the axial load and the subsequent trend of the fundamental natural frequency variation is shown in Fig. 3. The right-hand side of the figure which is for the compressive loads agreed with the one illustrated by Amba-Rao [33], within the plotting accuracy, whereas the left-hand side of the figure corresponding to tensile loads was further checked using BUNVIS-RG [34]. Clearly, as evident from Fig. 3, when the axial load approaches the critical buckling load, the fundamental natural frequency for each of the three boundary conditions tends to zero, indicating the duality between the vibration and buckling problems.

The next example is a cantilever stepped beam comprising two parts, as shown in Fig. 4. The first part AB has a flexural rigidity EI and length aL where a is a constant and L is the total length of the beam whereas the second part BC has a flexural rigidity k^2EI and length $L(1\text{-}a)$. (Note that k^2EI is taken as the flexural rigidity of the part BC only for convenience of presenting results.). The critical buckling load (P_{cr}) of the stepped beam was established for different values of a and k using the theory developed in Appendix C. For $k = 1$ and $0 < a < 1$, numerical results for the critical buckling load P_{cr} of the stepped column given by the theory of Appendix C reduced to the degenerate case of a uniform cantilever column verifying that $P_{cr} = \frac{\pi^2 EI}{4L^2}$ for $k = 1$. Now, representative results for

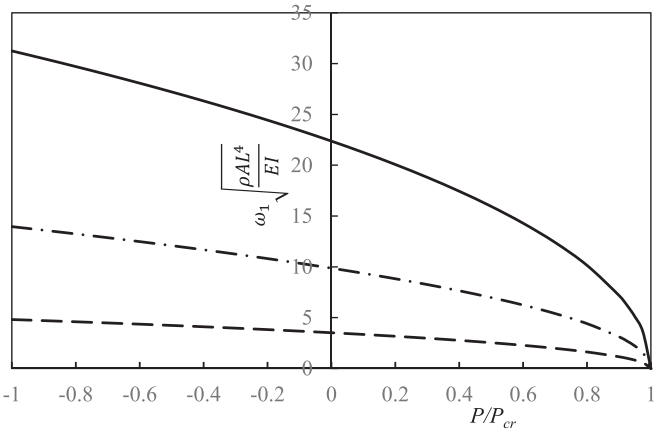

Fig. 3. The effect of axial load on the fundamental natural frequency of a Bernoulli Euler beam for different boundary conditions. ——— CC; - · - · - · - PP; – – – – CF.

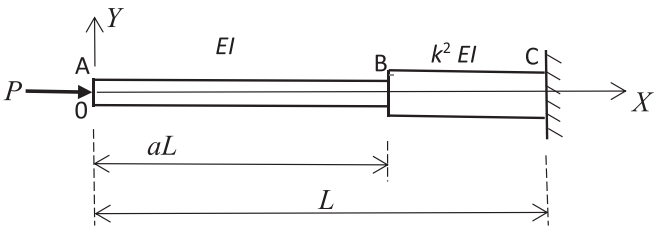

Fig. 4. A cantilever stepped beam under the action of a compressive axial load P.

$a = 0.5$ and 0.75, and $k = 1.5$ and 2 showing the non-dimensional critical buckling load are given in Table 2.

Although the results given in non-dimensional form in Table 2 are useful in that they can be applied universally, regardless of specific numerical values for a, k, EI and L in any unit, it would be instructive to give some numerical results in dimensional form, particularly for those interested readers who wish to develop the current theory further and wish to check their own computer programs. Thus, the illustrative example of the stepped beam shown Fig. 4 is given the following numerical data. The beam is made of steel with Young's modulus $E = 200$ GPa and density $\rho = 7850$ kg/m^3. Both parts AB and BC of the beam (see Fig. 4) are of solid circular cross-sections with diameters 0.02 m and 0.03 m, respectively, which gave $k = 2.25$. The length of the full beam L and the parameter a, are set to 1.25 m and 0.5, respectively. Using the

Table 2
Critical buckling load of a cantilever stepped column.

a	k	$P_{cr}/(\pi^2 EI/4L^2)$
0.5	1.5	1.8071
	2.0	2.4565
0.75	1.5	1.3426
	2.0	1.5114

Table 1
Fundamental natural frequency of an axially loaded beam for different boundary conditions.

Boundary conditions	Non-dimensional fundamental natural frequency $\left(\omega_1\sqrt{\frac{\rho AL^4}{EI}}\right)$								
	P/P_{cr}								
	−1.0	−0.8	−0.4	−0.2	0.0	0.2	0.4	0.8	1.0
CF	4.8147	4.5946	4.1032	3.8245	3.5160	3.1682	2.7652	1.6237	0.000
PP	13.958	13.241	11.678	10.812	9.8696	8.8276	7.6450	4.4138	0.000
CC	31.249	29.709	26.327	24.439	22.373	20.073	17.442	10.148	0.000

Table 3
Natural frequencies of stepped beam carrying tensile and compressive loads.

Natural frequency number (i)	Natural frequency ω_i (rad/s) P/P_{cr}								
	−0.8	−0.6	−0.4	−0.2	0.0	0.2	0.4	0.6	0.8
1	141.837	135.864	129.275	121.906	113.515	103.736	91.9559	77.0060	55.9705
2	474.235	463.052	451.479	439.491	427.066	414.181	400.818	386.963	372.613
3	1299.33	1288.79	1278.12	1267.33	1256.41	1245.37	1234.20	1222.90	1211.47
4	2335.06	2325.70	2316.31	2306.90	2297.44	2287.96	2278.45	2268.90	2259.32
5	4011.65	4001.87	3992.07	3982.23	3972.36	3962.46	3952.53	3942.56	3932.56

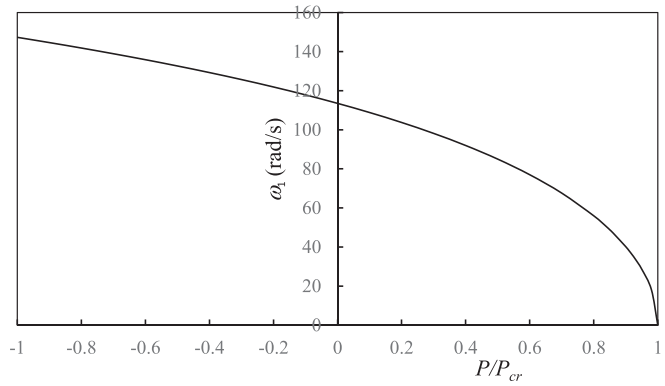

Fig. 5. Variation of the fundamental natural frequency (ω_1) of stepped beam against the axial load ratio (P/P_{cr}).

buckling theory given in Appendix C, the critical buckling load of the stepped beam was established at P_{cr}=6702.77 N. Next, the first five natural frequencies were computed using the current theory for a range of compressive and tensile loads expressed as fractions of the critical buckling load P_{cr}. Representative results are shown in Table 3. As expected, the natural frequencies increase with tensile load whereas they diminish with compressive loads.

The variation of the fundamental natural frequency of the cantilever stepped beam for a range of tensile and compressive loads is shown in Fig. 5. Clearly, the figure shows very similar trend observed for a uniformed beam (see Fig. 3). The fundamental natural frequency of the stepped cantilever beam reduces with compressive load and eventually becomes zero when buckling load is reached, i.e. when $P/P_{cr} = 1$, as shown in Fig. 5.

To validate the accuracy of the present theory, the stepped beam of Fig. 4 was further investigated by using FEM which relies on frequency-independent mass, elastic, and geometric stiffness matrices (see Appendix B). In the FEM analysis, 2, 4 and 10 element idealisations of the stepped beam were used to determine its natural frequencies. In the 2-element idealisation, each part of the beam (AB and BC) was treated as a single element whereas in the 4 and 10 element idealisations, each of the two parts was divided into 2 and 5 elements of equal lengths, respectively. Clearly, only 2 elements were needed in the present theory to achieve any desired accuracy because unlike FEM, the present theory

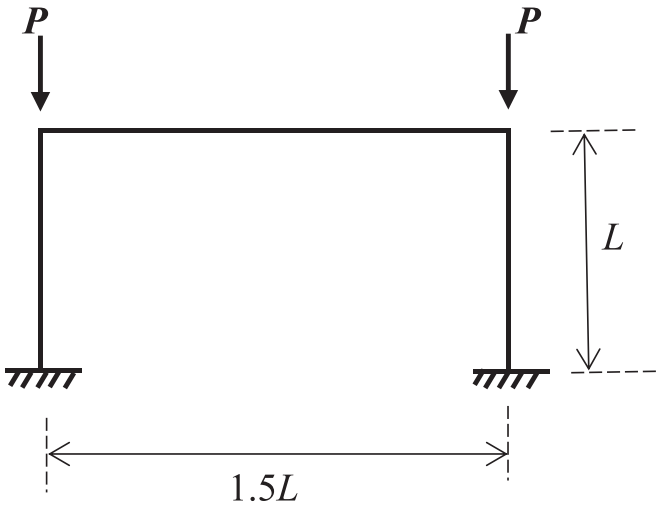

Fig. 6. A Portal frame.

is exact and thus, further discretisation of the stepped beam was unnecessary to improve the accuracy. The first five natural frequencies of the stepped beam using the present theory and the FEM are shown in Table 4 when both tensile and compressive forces in the stepped beam was set to 50 % of its critical buckling load P_{cr}.

As can be seen from Table 4, when 2-element idealisation was used ($N = 2$), FEM gave practically good results for the first two natural frequencies, but unacceptably poor results were generated by FEM for the 3rd, 4th and 5th natural frequencies. The accuracy of the 3rd and 4th natural frequency improved considerably when 4 elements were used, but the 5th natural frequency was not so accurate. However, when the number of element (N) was increased to 10 in the FEM analysis, almost comparable results with the present theory was achieved, as can be seen in Table 4. Although the first five natural frequencies computed using FEM for $N = 10$ agreed very well with those obtained from the present theory, it should nevertheless, be noted that in the much higher frequency range, FEM results are expected to be considerably less accurate and perhaps FEM might become unreliable. This is against the background that modal analysis in the high frequency range is often required as an important prerequisite in the statistical energy analysis (SEA) method. It is well-known that the modal density of structures in the high

Table 4
Comparative results using finite element method for natural frequencies of stepped cantilever beam of Fig. 4 (N = Number of elements used in the finite element method).

NaturalFrequency Number (i)	Natural frequency ω_i (rad/s) $P = 0.5P_{cr}$				$P = -0.5P_{cr}$			
	Current Theory	Finite Element Method $N = 2$	$N = 4$	$N = 10$	Current theory	Finite Element Method $N = 2$	$N = 4$	$N = 10$
1	84.990	85.012	84.993	84.990	132.66	133.03	132.68	132.66
2	393.95	396.92	394.42	393.96	457.32	460.16	457.88	457.33
3	1228.6	1568.8	1237.4	1228.9	1283.5	1618.7	1293.0	1283.9
4	2273.7	3535.0	2311.6	2275.8	2321.0	3603.6	2356.0	2323.2
5	3947.5	7374.7	4563.3	3958.8	3996.5	7374.7	4610.9	4008.2

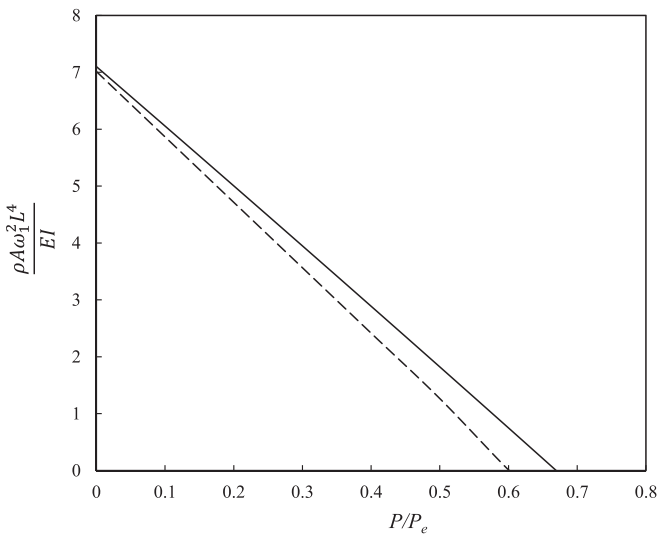

Fig. 7. The effect of loading on the fundamental natural frequency of portal frame. ———————— Current theory, – – – – – – – – – – – – – – – – Doyle [41].

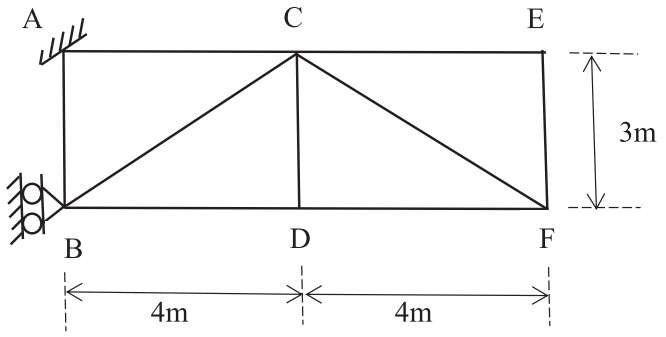

Fig. 8. A plane frame comprising axially loaded and unloaded beams for free vibration analysis using frequency-dependent mass, elastic, and geometric stiffness matrices.

frequency range is usually very high [35–38]. Furthermore, the need for high frequency vibration analysis of classical structures like beams with great accuracy is significant when carrying out energy flow analysis [39,40]. For such applications, the traditional FEM which is generally most effective within low and medium frequency range, may be totally inadequate.

The next set of results was computed for a portal frame shown in Fig. 6 for which the free vibration behaviour was investigated by Doyle [41] who by developing an approximate modification of the stiffness and carry-over factor for the axial load arrived at the frequency equation of the portal frame. The portal frame used by Doyle [41] is of single bay and single storey with each of the two columns (stanchions) has a length L and the beam has a length 1.5L. The flexural rigidity EI was taken to be constant throughout for all three members which were assumed to be inextensional, i.e., their axial or extensional rigidity (EA) considered to be infinite. From a computational point of view, when analysing the portal frame using the present theory, the axial rigidity (EA) for all three members was set to a very large number to make them inextensible so that results become directly comparable with those of Doyle [41].

To be consistent with the results presented by Doyle [41], the fundamental natural frequency of the portal frame shown in Fig. 6 was computed for a wide range of the ratio $R = P/P_e$ where P is the applied compressive load and P_e is the Euler load given by $P_e = \frac{\pi^2 EI}{L^2}$. It is intriguingly fascinating to note that by retaining only the first order terms, Doyle [41] managed to derive a linear relationship between the square of the non-dimensional fundamental natural frequency $\bar{\omega}_1 = \omega_1\sqrt{\frac{\rho AL^4}{EI}}$ of the portal frame and the load ratio P/P_e. The relationship is approximate, but nevertheless, very useful to provide some practical estimate of the fundamental natural frequency. The relationship is given by (see Doyle's equation (36))

$$\frac{R}{0.61} + \frac{\bar{\omega}_1^2}{7.015} = 1 \tag{85}$$

Doyle [41] plotted $\bar{\omega}_1^2$ against P/P_e and showed the linear relationship by a straight line joining the coordinates (0, 7.015) and (0.61, 0) in his graph, see his Fig. 4. (Note that there is a typographical error in Doyle's figure in that the horizonal axis should be labelled P/P_e instead of P.) By applying the exact theory of this paper, the plot of $\bar{\omega}_1^2$ against P/P_e is shown in Fig. 7 alongside the graph of Doyle [41]. For the portal frame analysed, Doyle's relationship between the fundamental natural frequency ($\bar{\omega}_1$) and the load ratio (P/P_e) appears to have worked reasonably well for lower values of P/P_e ratio, but the error increases for larger values of the ratio P/P_e as evident from Fig. 7.

The final illustrative example is that of a plane frame shown in Fig. 8 with its principal dimensions. The node at A is fully fixed, i.e., built-in whereas the node at B has a roller support which prevents horizonal motion but allows vertical motion and rotation. The rest of the nodes are free. Each of the nine members of the frame has the same bending rigidity $EI = 5 \times 10^6$ Nm^2, axial rigidity $EA = 9 \times 10^8$N and mass per unit length $\rho A = 35$ kg/m. The horizontal members AC, BD, CE and DF carry a compressive axial force of 4EI/l^2, the diagonal members BC and CF carry a tensile axial force of 5EI/l^2, where l is the length of the member concerned, and the vertical members AB, CD and EF are unloaded. The first five natural frequencies of the frame were computed applying the frequency dependent mass, elastic and geometric stiffness matrices developed in this paper. These natural frequencies were also computed by using the commercial FEM software ABAQUS [42]. When computing the FEM results using ABAQUS, 9, 20, 35, 70 and 140 element idealisations were used. In the 9-element idealisation, each member (beam) of the frame was a single element. Then, each member was split into several elements of equal lengths so that the total number of elements used (N) in the analysis were 20, 30, 70 and 140, respectively. For N = 20, each of the horizonal members (AC, CE, BD and DF) were divided into 2 elements, each of the vertical members (AB, CD and EF) were divided into 2 elements and each of the diagonal members (BC and CF) were divided into 3 elements. The corresponding numbers for the discretisation of the horizontal, vertical and diagonal members were 4, 3 and 5 for $N = 35$; 8, 6 and 10 for $N = 70$; and 16, 12 and 20 for $N = 140$.

Table 5
Natural frequencies of plane frame using current theory and ABAQUS [42] (N = Number of elements used in ABAQUS).

Natural frequency number (i)	Natural Frequencies ω_i (rad/s)					
	Current Theory	ABAQUS Results				
		$N = 9$	$N = 20$	$N = 35$	$N = 70$	$N = 140$
1	159.03	166.34	160.85	160.69	160.67	160.67
2	259.26	376.60	270.57	269.90	269.81	269.81
3	297.59	395.73	313.04	311.66	311.53	311.52
4	324.49	526.14	362.51	360.22	360.00	360.00
5	406.47	603.68	428.76	424.27	423.94	423.93

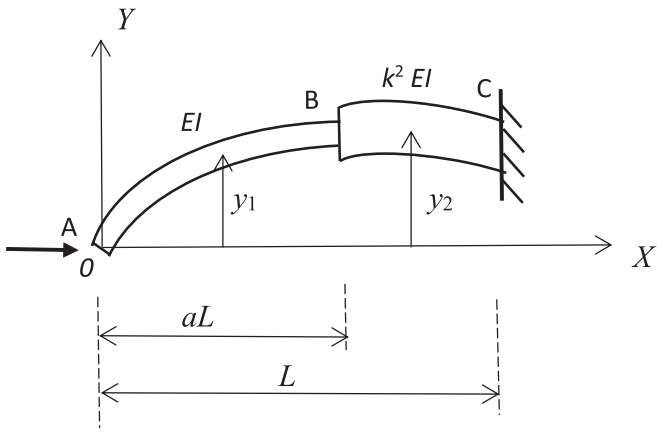

Fig. C1. Deflected shape of the stepped beam shown in Fig. 4.

respectively. The first five natural frequencies of the frame using the present theory and ABAQUS [42] are shown in Table 5.

The results of Table 5 indicate that 9-element idealisation in ABAQUS ($N = 9$) gives 4.6 % error in the fundamental natural frequency when compared with the exact result of the current theory which also used 9 elements in the analysis, but the errors incurred in the 2nd, 3rd, 4th and 5th natural frequencies using ABAQUS are 45.3 %, 33 %, 62 % and 48.5 %, respectively. This is unacceptably bad. When 20-element idealisation was used the errors in the five natural frequencies diminished to 1.14 %, 4.36, 5.22 %, 11.7 % and 5.48 %, respectively. As expected, with increasing number of elements, the results gradually converged towards exact results of the current theory, and $N = 140$ gave sufficiently close results, see Table 5. Clearly in the high frequency range, finite element results will be considerably less accurate and may not be suitable for statistical energy analysis [35–38]. The exact results of Table 5 have been further validated by the computer program BUNVIS-RG [34] based on the dynamic stiffness method.

8. Conclusions

Through rigorous application of symbolic computation, the frequency-dependent mass, elastic, and geometric stiffness matrices of an axially loaded Bernoulli-Euler beam have been derived and their relationship with the corresponding dynamic stiffness matrix has been established. The investigation allows exact free vibration analysis of axially loaded beams and frameworks, but importantly, it paves the way for the inclusion of damping, e.g., proportional or modal damping, in exact free vibration analysis of such structures using the dynamic stiffness method, which has not been possible before. Several illustrative examples by applying the Wittrick-Williams algorithm are given to demonstrate the capability of the theory which has been verified by finite element results.

Declaration of competing interest

The authors declare that they have no known competing financial interests or personal relationships that could have appeared to influence the work reported in this paper.

Data availability

Data will be made available on request.

Acknowledgement

The author is grateful to EPSRC, UK for an earlier grant (GR/R21875/01) and to Leverhulme Trust, UK for a recent grant (EM-2019-061) which made this work possible. The author thankfully appreciates the help given by Professor Alfonso Pagani, Department of Mechanical and Aerospace Engineering, Polytechnic of Turin, Italy (who was his former PhD student at City, University of London) when computing the ABAQUS results.

Appendix A. Frequency-dependent mass and stiffness matrices of a beam in axial motion

The frequency-dependent mass and stiffness matrices of a beam in axial motion are available in the literature [1,7] and therefore, the details of their derivation are not given here, but the final results for the two matrices $\mathbf{m}^{\mathbf{a}}(\omega)$ and $\mathbf{k}^{\mathbf{a}}(\omega)$ of the beam with axial rigidity EA, mass per unit length ρA and length L, are given below. Note that these matrices in axial motion can be combined with the corresponding matrices in flexural motion derived in Sections 3-5.

$$\mathbf{m}^{\mathbf{a}}(\omega) = \begin{bmatrix} m^a_{11} & m^a_{12} \\ m^a_{21} & m^a_{22} \end{bmatrix} \tag{A1}$$

$$\mathbf{k}^{\mathbf{a}}(\omega) = \begin{bmatrix} k^a_{11} & k^a_{12} \\ k^a_{21} & k^a_{22} \end{bmatrix} \tag{A2}$$

where

$$m^a_{11}(\omega) = m^a_{22}(\omega) = \frac{\rho ALc}{2\omega}\operatorname{cosec}\frac{\omega}{c}\left(\frac{\omega}{c}\operatorname{cosec}\frac{\omega}{c} - \cos\frac{\omega}{c}\right) \tag{A3}$$

$$m^a_{12}(\omega) = m^a_{21}(\omega) = \frac{\rho ALc}{2\omega}\operatorname{cosec}\frac{\omega}{c}\left(1 - \frac{\omega}{c}\cot\frac{\omega}{c}\right) \tag{A4}$$

$$k^a_{11}(\omega) = k^a_{22}(\omega) = \frac{EA\omega}{2Lc}\operatorname{cosec}\frac{\omega}{c}\left(\frac{\omega}{c}\operatorname{cosec}\frac{\omega}{c} + \cos\frac{\omega}{c}\right) \tag{A5}$$

$$k^a_{12}(\omega) = k^a_{21}(\omega) = -\frac{EA\omega}{2Lc}\operatorname{cosec}\frac{\omega}{c}\left(1 + \frac{\omega}{c}\cot\frac{\omega}{c}\right) \tag{A6}$$

with c given by

$$c^2 = \frac{EA}{\rho AL^2} \tag{A7}$$

Appendix B. Frequency-independent mass, elastic and geometric stiffness matrices

Referring to Fig. 1, the frequency-independent mass ($\mathbf{m_0}$), elastic ($\mathbf{k_0^E}$) and geometric ($\mathbf{k_0^G}$) stiffness matrices for a beam that are generally used in the finite element method are given in the usual notation by [1]

$$\mathbf{m}_0 = \frac{\rho AL}{420}\begin{bmatrix} 156 & 22L & 54 & -13L \\ 22L & 4L^2 & 13L & -3L^2 \\ 54 & 13L & 156 & -22L \\ -13L & -3L^2 & -22L & 4L^2 \end{bmatrix} \tag{B1}$$

$$\mathbf{k}_0^{\mathbf{E}} = \frac{EI}{L^3}\begin{bmatrix} 12 & 6L & -12 & 6L \\ 6L & 4L^2 & -6L & 2L^2 \\ -12 & -6L & 12 & -6L \\ 6L & 2L^2 & -6L & 4L^2 \end{bmatrix}; \quad \mathbf{k}_0^{\mathbf{G}} = -\frac{P}{L}\begin{bmatrix} \frac{6}{5} & \frac{L}{10} & -\frac{6}{5} & \frac{L}{10} \\ \frac{L}{10} & \frac{2}{15}L^2 & -\frac{L}{10} & -\frac{L^2}{30} \\ -\frac{6}{5} & -\frac{L}{10} & \frac{6}{5} & -\frac{L}{10} \\ \frac{L}{10} & -\frac{L^2}{30} & -\frac{L}{10} & \frac{2}{15}L^2 \end{bmatrix} \tag{B2}$$

The corresponding frequency-independent mass and stiffness matrices in axial motion (i.e., those for a bar element) given below are to be incorporated into Eqs. (B1)–(B2) so that frameworks can be analysed for their free vibration characteristics.

$$\mathbf{m}_0^{\mathbf{A}} = \frac{\rho AL}{6}\begin{bmatrix} 2 & 1 \\ 1 & 2 \end{bmatrix}; \quad \mathbf{k}_0^{\mathbf{A}} = \frac{EA}{L}\begin{bmatrix} 1 & -1 \\ -1 & 1 \end{bmatrix} \tag{B3}$$

The computation of natural frequencies for a frame is generally achieved by assembling the element mass, elastic and geometric stiffness matrices in the frame in global or datum coordinates by using standard coordinate transformation technique and then applying the usual eigensolution procedure employed in the finite element method for the equation $\mathbf{K^E} + \mathbf{K^G} - \omega^2\mathbf{M} = 0$ where $\mathbf{K^E}$, $\mathbf{K^G}$, and $\mathbf{M}$ are respectively the overall elastic and geometric stiffness and mass matrices of the complete frame.

Appendix C. Critical buckling load of a stepped cantilever column

The critical buckling load of the stepped cantilever column shown in Fig. 4 is determined theoretically in this appendix. The deflected shape of the column is shown below in Fig. C1. The co-ordinate system (XY) which is fixed at the origin O at the tip is allowed to move vertically up and down, but its rotation and horizontal movements are not allowed.

Let the flexural displacements of the column in the two parts AB and BC at some given points be, respectively y_1 and y_2. Now, these are considered separately, allowing two separate slopes.

The governing differential equation for the first part AB, i.e., along the left section is given by

$$\text{Bending moment}: M = Py_1 = -EI\frac{d^2y_1}{dx^2} \tag{C1}$$

The solution in the usual form is obtained as

$$y_1 = A_1\sin\lambda x + B_1\cos\lambda x \tag{C2}$$

where

$$\lambda = \sqrt{\frac{P}{EI}} \tag{C3}$$

The bending moment at $x = 0$ implies $y_1''(0) = 0$ which from Eq. (C2) gives

$$B_1 = 0 \tag{C4}$$

Thus, from Eq. (C2)

$$y_1 = A_1\sin\lambda x \tag{C5}$$

The governing differential equation for the second part BC along the right section is given by

$$\text{Bending moment}: M = Py_2 = -k^2EI\frac{d^2y_2}{dx^2} \tag{C6}$$

The solution is

$$y_2 = A_2\sin\frac{\lambda x}{k} + B_2\cos\frac{\lambda x}{k} \tag{C7}$$

The slope at the cantilever end ($x = L$) is zero means $y_2'(L) = 0$ from which Eq. (C7) gives

$$A_2 = B_2 \tan\frac{\lambda L}{k} \tag{C8}$$

Thus, from Eq. (C7)

$$y_2 = B_2\left(\tan\frac{\lambda L}{k}\sin\frac{\lambda x}{k} + \cos\frac{\lambda x}{k}\right) \tag{C9}$$

Now, at $x = aL$, y_1 must be equal to y_2 and $y_1^{'}$ and $y_2^{'}$ also be equal to satisfy the continuity conditions for displacement and slope at B (see Fig. C1). These continuity conditions give

$$A_1 \sin\lambda aL = B_2\left(\tan\frac{\lambda L}{k}\sin\frac{\lambda aL}{k} + \cos\frac{\lambda aL}{k}\right) \tag{C10}$$

and

$$A_1 \lambda\cos\lambda aL = B_2\frac{\lambda}{k}\left(\tan\frac{\lambda L}{k}\cos\frac{\lambda aL}{k} - \sin\frac{\lambda aL}{k}\right) \tag{C11}$$

Equations (C10) and (C11) can be written in the following matrix form

$$\begin{bmatrix} \sin\lambda aL & -\left(\tan\frac{\lambda L}{k}\sin\frac{\lambda aL}{k} + \cos\frac{\lambda aL}{k}\right) \\ \lambda\cos\lambda aL & -\frac{\lambda}{k}\left(\tan\frac{\lambda L}{k}\cos\frac{\lambda aL}{k} - \sin\frac{\lambda aL}{k}\right) \end{bmatrix} \begin{bmatrix} A_1 \\ B_2 \end{bmatrix} = 0 \tag{C12}$$

For a non-trivial solution, the 2×2 determinant of the above matrix must be zero, yielding the following buckling equation

$$\tan\lambda aL = \frac{k\left(\tan\frac{\lambda L}{k}\sin\frac{\lambda aL}{k} + \cos\frac{\lambda aL}{k}\right)}{\left(\tan\frac{\lambda L}{k}\cos\frac{\lambda aL}{k} - \sin\frac{\lambda aL}{k}\right)} \tag{C13}$$

For different values of the combination of a and k, Eq. (C13) can be solved to determine λL through an iterative process so that the critical buckling load P_{cr} can be obtained with the help of Eq. (C3).

The degenerate case for a uniform cantilever column can be obtained by substituting $k = 1$ and $a = 0$ in Eq. (C13) to give

$$0 = \frac{1}{\tan\lambda L} \tag{C14}$$

or

$$\tan\lambda L = \infty = \tan\frac{\pi}{2} \tag{C15}$$

or

$$\lambda^2 = \frac{\pi^2}{4L^2} \tag{C16}$$

Substituting λ from Eq. (C3) into Eq. (C16) yields the critical buckling load $P_{cr} = \frac{\pi^2 EI}{4L^2}$ which is the well-known result for a cantilever column that can be found in standard texts.

References

[1] Przemieniecki JS. Theory of matrix structural analysis. Dover Publications Inc; 1985.
[2] Downs B. Vibration analysis of continuous systems by dynamic discretization. ASME J Mech Design 1980;102:391–8. https://doi.org/10.1115/1.3254757.
[3] Melosh RJ, Smith HA. New formulation for vibration analysis. ASCE J Eng Mech 1989;115(3):543–54. https://doi.org/10.1061/(ASCE)0733-9399(1989)115:3(543).
[4] Fergusson NJ, Pilkey WD. Frequency-dependent element mass matrices. J Appl Mech 1992;59(1):136–9. https://doi.org/10.1115/1.2899418.
[5] Paz M, Dung L. Power series expansion of the general stiffness matrix for beam elements. Int J Num Meth Eng 1975;9(2):449–59. https://doi.org/10.1002/nme.1620090212.
[6] Dumont NA, de Oliveira R. From frequency-dependent mass and stiffness matrices to the dynamic response of elastic systems. Int J Solids Struct 2001;38(10–13):1813–30. https://doi.org/10.1016/S0020-7683(00)00137-2.
[7] Banerjee JR. Frequency dependent mass and stiffness matrices of bar and beam elements and their equivalency with the dynamic stiffness matrix. Comput Struct 2021;254:p106616. https://doi.org/10.1016/j.compstruc.2021.106616.
[8] Sathyamoorthy M, Sirigiri R. Structural analysis of box beams using symbolic manipulation technique. J Aircraft 1993;30(2):262–7. https://doi.org/10.2514/3.48275.
[9] Beltzer AI. Engineering analysis via symbolic computation-a breakthrough. Appl Mech Reviews 1990;43:119–27. https://doi.org/10.1115/1.3119164.
[10] Pavlovic MN. Symbolic computation in structural engineering. Comput Struct 2003;81(22–23):2121–36. https://doi.org/10.1016/S0045-7949(03)00286-4.
[11] Banerjee J.R. An exact analytical method of flutter analysis using symbolic computation. In: Proceed 40th AIAA/ASME/ASCE/AHS/ASC Structures, Structural Dynamics, and Materials Conference; 1999. Paper No. AIAA-99-1354. doi: 10.2514/6.1999-1354.
[12] Banerjee JR. Exact modal analysis of an idealised whole aircraft using symbolic computation. Aeronaut J 2000;104:247–55. https://doi.org/10.1017/S0001924000091545.
[13] Banerjee JR. Explicit modal analysis of axially loaded composite Timoshenko beams using symbolic computation. J Aircraft 2002;39(5):909–12. https://doi.org/10.2514/2.3018.
[14] Banerjee JR, Sobey AJ, Su H, Fitch JP. Use of computer algebra in Hamiltonian calculations. Adv Eng Software 2008;39(6):521–5. https://doi.org/10.1016/j.advengsoft.2007.03.013.
[15] Wittrick WH, Williams FW. A general algorithm for computing natural frequencies of elastic structures. Quart J Mech Appl Math 1971;24(3):263–84. https://doi.org/10.1093/qjmam/24.3.263.
[16] Kolousek V. Dynamics in Engineering Structures. London: Butterworth; 1973.
[17] Williams FW, Wittrick WH. Exact buckling and frequency calculations surveyed. J Struct Eng 1983;109(1):169–87. https://doi.org/10.1061/(ASCE)0733-9445(1983)109:1(169).
[18] Williams FW. Review of exact buckling and frequency calculations with optional multi-level substructuring. Comput Struct 1993;48(3):547–52. https://doi.org/10.1016/0045-7949(93)90334-A.

[19] Banerjee JR. The dynamic stiffness method: theory, practice and promise. Computational Technology Reviews, Saxe-Coburg Publications 2015;11(1):31–57. https://doi.org/10.4203/ctr.11.2.
[20] Banerjee JR. Review of the dynamic stiffness method for free vibration analysis of beams. Transport Safety Environ 2019;1(2):106–16. https://doi.org/10.1093/tse/tdz005.
[21] Naprstek J, Fischer C. Static and dynamic analysis of beam assemblies using a differential system on an oriented graph. Comput Struct 2015;155:28–41. https://doi.org/10.1016/j.compstruc.2015.02.021.
[22] Naprstek J, Fischer C. Investigation of bar system modal characteristics using dynamic stiffness matrix polynomial approximations. Comput Struct 2017;180:3–12. https://doi.org/10.1016/j.compstruc.2016.10.015.
[23] Lee SW, Kim YH. A new approach to the finite element modelling of beams with warping effect. Int J Num Meth Eng 1987;24(12):2327–41. https://doi.org/10.1002/nme.1620241207.
[24] Wei G, Lardeur P, Druesne, F. A new solid-beam approach based on first or higher-order beam theories for finite element analysis of thin to thick structures. Finite Elem Analy Des 2022;200: Paper 103655. https://doi.org/10.1016/j.finel.2021.103655.
[25] Xie L, Wang S, Ding J, Banerjee J.R, Wng J. An accurate beam theory and its first-order approximation in free vibration analysis. J Sound Vib 2020; 485: Paper 115567. https://doi.org/10.1016/j.jsv.2020.115567.
[26] Fazzolari A. A beam formulation with 3D capabilities for the free vibration analysis of thin-walled metallic and composite structures. Thin-Walled Struct 2020;146: Paper 106441. https://doi.org/10.1016/j.tws.2019.106441.
[27] Augello R, Daneshkhah E, Xu X, Carrera E. Efficient CUF-based method for the vibrations of thin-walled open cross-section beams under compression. J Sound Vib 2021; 510: Paper 116232. https://doi.org/10.1016/j.jsv.2021.116232.
[28] Filippi M, Pagani A, Carrera E. High-order finite beam elements for propagation analyses of arbitrary-shaped one-dimensional waveguides. Mech of Adv Mat and Struct 2022;29(13):1883–91. https://doi.org/10.1080/15376494.2020.1842951.
[29] Zienkiewicz OC, Taylor RL, Zhu JZ. The finite element method: its basis and fundamentals. 7th edition. Elsevier; 2013.
[30] Bathe KJ. Finite element procedures in engineering analysis. Prentice-Hall; 1982.
[31] Fitch JP. Solving algebraic problems with REDUCE. J Symb Comput 1985;1(2):211–27. https://doi.org/10.1016/S0747-7171(85)80015-8.
[32] Hearn AC. REDUCE user's manual version 3.8. Santa Monica, CA, USA; 2004.
[33] Amba-Rao CL. Effect of end conditions on the lateral frequencies of uniform straight columns. J Acoust Soc Amer 1967;42(4):900–1. https://doi.org/10.1121/1.1910667.
[34] Anderson MS, Williams FW, Banerjee JR, Durling BJ, Herstorm CL, Kennedy D, et al. User manual for BUNVIS-RG: an exact buckling and vibration program for lattice structures, with repetitive geometry and substructuring options. NASA Tech Memo 1986;87669.
[35] Lyon RH. Statistical energy analysis of dynamical Systems: theory and applications. USA: MIT Press, Cambridge; 1975.
[36] Fahy F. Statistical energy analysis: a critical overview. Philo Trans: Phys Sci Eng, The Royal Society 1994;346(1681):431–47. https://doi.org/10.1098/rsta.1994.0027.
[37] Lyon RH, DeJong RG. Theory and application of statistical energy analysis. second edition. London, UK: Butterworth-Heinermann; 1995.
[38] Keane AJ, Price WC. Statistical energy analysis: An overview, with applications in structural dynamics. UK: Cambridge University Press; 1997.
[39] Wohlever JC, Bernhard RJ. Mechanical energy flow models of rods and beams. J Sound Vib 1992;153:1–19. https://doi.org/10.1016/0022-460X(92)90623-6.
[40] Lase Y, Ichchou MN, Jezequel L. Energy flow analysis of bars and beams: Theoretical formulations. J Sound Vib 1996;192:281–305. https://doi.org/10.1006/jsvi.1996.0188.
[41] Doyle JF. Approximate modifications of stiffness and carry-over factors for axial loads and vibrations. Struct Engineers 1973;51(5):183–7.
[42] Abaqus. Dassault Systemes Simuli Corporation. RI, USA: Providence; 2021.